Optoelectronic Properties of Solution Grown ZnO n-p or p-n Core–Shell Nanowire Arrays

Ken C. Pradel,[†] Yong Ding,[†] Wenzhuo Wu,[†] Yoshio Bando,[‡] Naoki Fukata,*,[‡] and Zhong Lin Wang*,[†,‡]

[†]School of Materials Science and Engineering, Georgia Institute of Technology, Atlanta, Georgia 30332-0245, United States
[‡]International Center for Materials Nanoarchitectonics, National Institute for Materials Science, 1-1 Namiki, Tsukuba, 305-0044, Japan

S *Supporting Information*

ABSTRACT: Sb doped ZnO nanowires grown using the low-temperature hydrothermal method have the longest reported p-type stability of over 18 months. Using this growth system, bulk homojunction films of core–shell ZnO nanowires were synthesized with either n or p-type cores and the oppositely doped shell. Extensive transmission electron microscopy (TEM) characterization showed that the nanowires remain single crystalline, and the previously reported signs of doping remain intact. The electronic properties of these films were measured, and ultraviolet photo-detection was observed. This growth technique could serve as the basis for other optoelectronic devices based on ZnO such as light emitting diodes and photovoltaics.

KEYWORDS: *p-type ZnO, homojunction, core–shell nanowire, photodetection, hydrothermal growth*
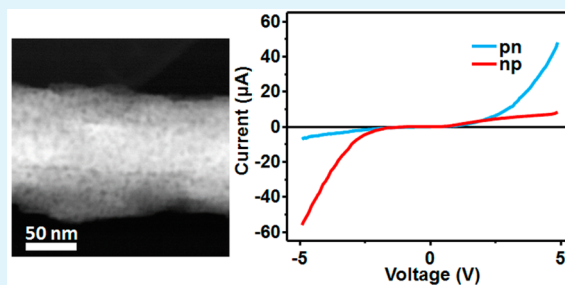
Core–shell nanowire structures have often been of interest for optoelectronics due to their high interfacial area, allowing for more electron–hole formation or recombination.[1–3] Zinc oxide in particular has been a popular material for optoelectronic research due to its ease of synthesis, low cost, and wide direct band gap. Numerous heterojunction structures with ZnO have been demonstrated using materials such as ZnSe,[4,5] Fe_3O_4,[6] TiO_2,[7] and Al_2O_3[8] for applications in both light emission and photosensing. However, a homojunction structure would be preferred as it reduces the lattice mismatch between the two components. There have been a number of reports on zinc oxide axial[9–11] p-n homojunctions and even a few on core–shell[12–15] structures as well. While these works have presented promising results, the possibility of p-type ZnO has long been the subject of debate. ZnO is notoriously difficult to make p-type due to the presence of intrinsic donor defects during synthesis such as zinc or hydrogen interstitials, and potentially oxygen vacancies, causing the material to become naturally n-type.[16,17] While there have been numerous reports on successful p-type doping of ZnO,[18–20] few mention the stability and lifetime of the material. Therefore, finding an appropriate dopant is of utmost importance.

Recently, it was shown that antimony, a relatively heavy element compared to zinc and oxygen, makes for a stable dopant, with p-type behavior remaining stable for at least 18 months.[21,22] Furthermore, this p-type material can be synthesized at temperatures less than 100 °C in aqueous solution, allowing for applications in flexible electronics. Further studies have shown that modifying the growth solution allows for novel structures such as ultralong nanowires or densely packed films[23,24] demonstrating applications in nano-generators[25–27] and piezotronics.[28,29] In this work, zinc oxide core–shell homojunction nanowires are synthesized using a low temperature hydrothermal method. Core–shell wires could be grown with either n-type or p-type cores with the oppositely doped shell. The electrical properties of these structures were measured, and the resulting structure were shown to have photoresponse in the ultraviolet range.

Core–shell structures were grown based on previously demonstrated nanowire growth techniques. The following process is shown schematically in Figure 1a. Glass substrates were chosen as substrates, and 100 nm of aluminum doped zinc oxide (AZO) was sputtered on to act as a seed layer and bottom electrode for subsequent electrical measurements. Previous work has shown that AZO will form an Ohmic contact with both n- and p-type ZnO, making it an ideal choice for the seed layer.[24] A 2:1 ratio of zinc nitrate to hexamethylenetetramine (HMTA), respectively, were used for nanowire synthesis. All chemicals were purchased from Sigma-Aldrich and used as is without further purification. Using a zinc concentration of 5 mM produced well dispersed fine nanowires, which served as the core. To produce p-type nanowires, antimony glycolate solution was added in a molar ratio of 1% relative to zinc. Preparation of the dopant solution is described in detail in previous literature.[21] In both cases, 0.4 M ammonium hydroxide was added to the solution in order to
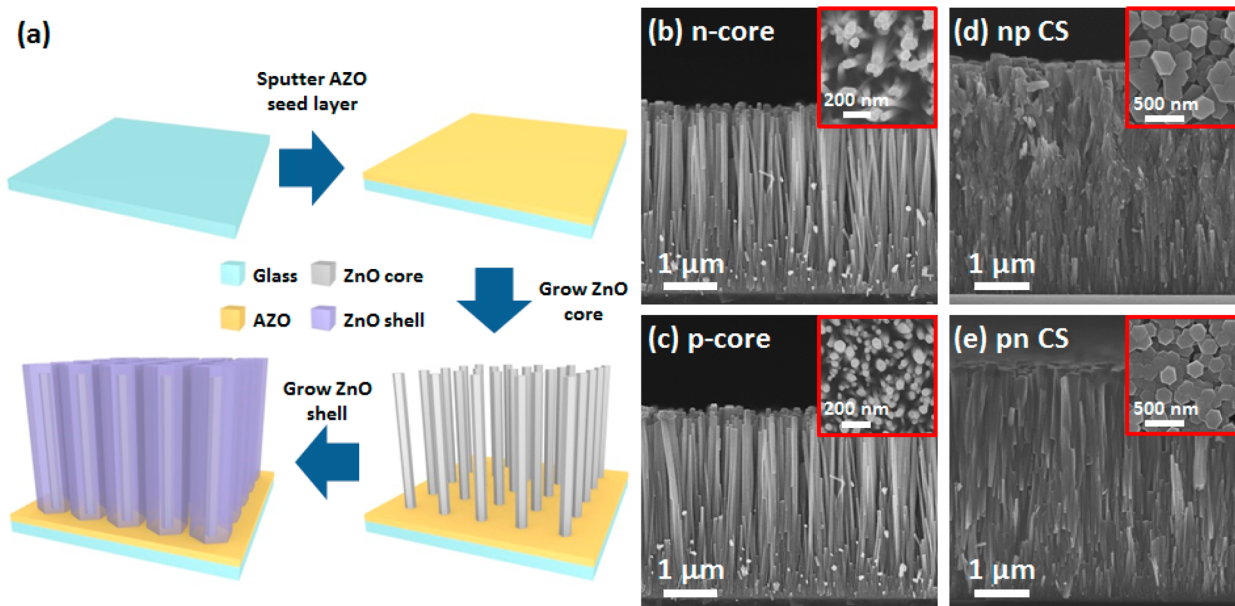
Figure 1. (a) Schematic representation of growth of core−shell nanowires. (b) n and (c) p-type fine core nanowires grown through the hydrothermal method. (d)**np** and (e)**pn** core−shell bulk homojunction arrays following shell layer growth. The insets show the top view of the nanowires.
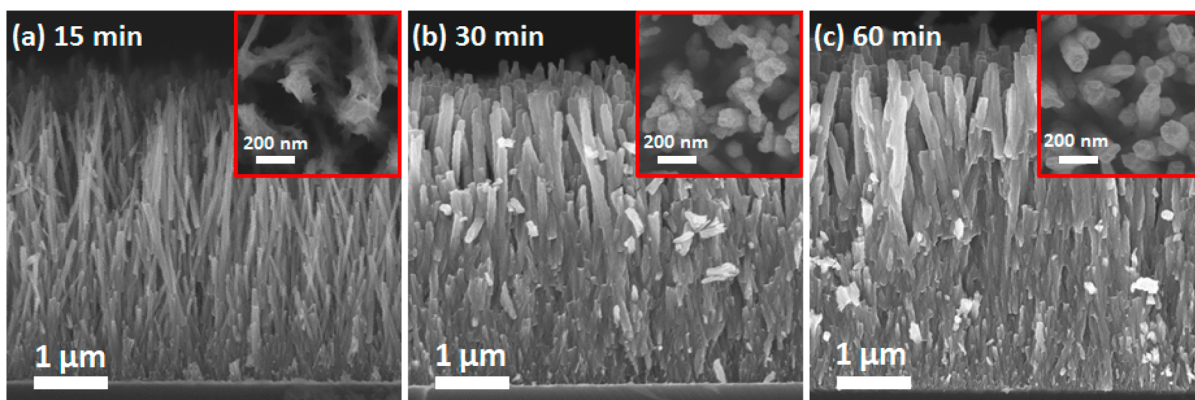

Figure 2. Growth progress of the shell layer for the **np** structure as a function of time for (a) 15, (b) 30, and (c) 60 min. The inset shows a top view of the sample.

help prevent homogeneous nucleation, thus promoting more uniform nanowire growth, and the substrate was floated face down on the solution surface and placed in an oven at 95 °C for 2 h. After growth, the substrates were removed from the solution and placed into a new solution to grow the shell layer. For the shell layer, a higher concentration of the precursors was used, 25 mM and 12.5 mM zinc nitrate and HMTA, respectively, for n-type shell, and 50 mM and 25 mM for the p-type. This was done as the addition of the dopant interferes with normal nanowire growth, so a higher concentration is needed in order to form a dense film. Sodium citrate was also added to the solution (0.7 mM for n-type, 1.4 mM for p-type) in order to suppress axial growth and promote radial growth.[30] 0.5 M ammonium hydroxide was added to the solution and the shell layer was grown at 75 °C for up to 2 h. Before optoelectronic measurements were performed, 100 nm of ITO were deposited on top of the film surface to act as the top electrode, and copper wires were attached to the electrodes using silver paste.

Scanning electron microscopy was performed using a Hitachi SU8010 field emission scanning electron microscope. Transmission electron microscopy was performed using a Tecnai F30 Analytical TEM. All electrical measurement were performed using a Keithley 4200 Semiconductor Characterization System. An AS ONE ultraviolet lamp with wavelengths of 254 and 365 nm was used as a light source. The measured power levels were 1.61 and 0.66 mW/cm^2 for each wavelength, respectively.

As can be observed from the SEM images (Figure 1b,c), the core nanowires have a uniform dimensions of about 3 μm in length and 50 nm in diameter regardless of the doping state. From the top view (inset), the wires are fairly well spaced, which will allow space for the shell layer to grow in between. Some bundling of the nanowires can be observed which likely happens due to the evaporation of water when the nanowires are removed from the growth solution. Following the growth of the shell layer, the nanowire diameter and density increased dramatically, causing them to grow until they impinged upon each other forming a bulk homojunction film (Figure 1d,e). Because sodium citrate slows down axial growth of zinc oxide
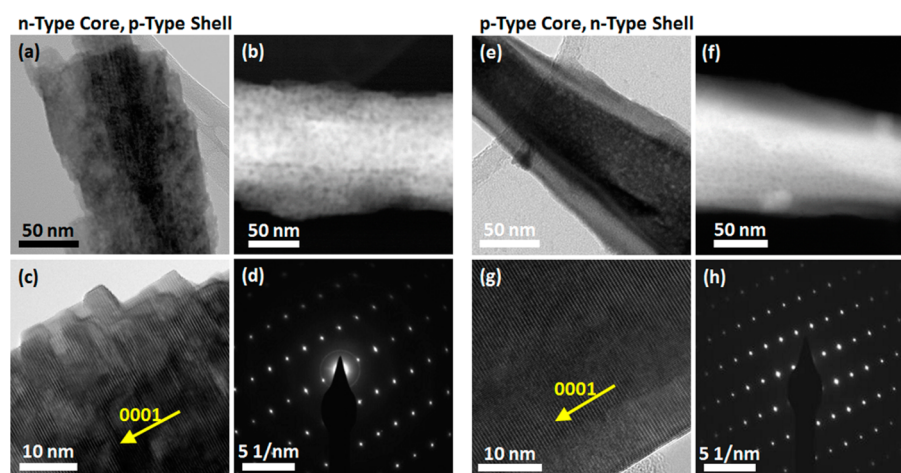
Figure 3. (a) Bright field TEM image of an **np** core−shell nanowire. The core is visible as the dark region in the center. (b) STEM image of the n-p nanowire. The core is visible as the bright while core, while a porous shell can be seen consistent with previous reports on Sb doped ZnO. (c) High-resolution TEM image of the shell layer. The structure still appears to be single crystalline, and the porosity is visible. (d) From the SAED, the nanowire is single crystalline despite the multiple growth steps. (e) Bright field TEM image of the p-n core−shell nanowire. The porosity caused by Sb is visible exclusively in the core layer. (f) STEM image of the core−shell wire. While the porosity is visible, the contrast is reduced due to the presence of the uniform shell layer. (g) HRTEM image of the core−shell nanowire. (h) The SAED pattern confirms that the nanowire is single crystalline in this growth scheme as well.

nanowires, the increase in length is minimized, and the film thickness increases by only about 1 μm. For the sake of brevity, n-type core and p-type shell nanowires will be referred to as **np** nanowires and p-type core, n-type shell nanowires will be **pn** wires. From the cross sectional view, the **np** film appears to have a rougher appearance, except at the base where the core nanowires are still partially visible. This appearance is consistent with previously demonstrated p-type films shown in the literature.[24] Because Sb is a much larger atom than Zn or O, it interferes with normal growth, causing a rougher appearance. This can be confirmed by comparing densely packed nanowire films grown using the same growth solution (Figure S-1). In order to get a better idea of the growth process, the **np** sample was grown for shorter periods of time (Figure 2). After only 15 min of growth (Figure 2a), some roughness is seen on the nanowire surface as the shell layer begins to grow, but there is not much change in the diameter. As the growth progresses to 30 min (Figure 2b), the nanowires begin to regain their hexagonal structure and become completely hexagonal again by 60 min (Figure 2c). As the shell layer grows, the wires become increasingly densely packed starting at the base and continuing until the tip. From the cross-sectional view, the length remains constant over the first 30 min and begins to grow longer after 60 min when most of the spacing near the base is filled in.

In order to characterize these structures, transmission electron microscopy (TEM) and scanning transmission electron microscopy (STEM) were used. For the purposes of microscopy, the shell layer was only grown for 15 min, as clear images of the microstructure cannot be obtained if the nanowire diameter is too thick. From the TEM image (Figure 3a), an obvious difference in contrast between the core and shell layers can be observed. In the **np** nanowire, porosity is clearly visible in the shell layer. This is characteristic of antimony doped ZnO nanowires. Because a high concentration of dopant was used, a large number of small pores form in the nanowire.[23] Because of its much larger atomic radius, the Sb atoms interfere with normal nanowire growth. The antimony forms plate-like precipitates in the nanowire, ZnO cannot

continue to grow on top of it, and so it grows around it, causing voids to form in the structure.[22] These voids become even clearer in the dark field STEM image in Figure 3b. The n-type core can be easily differentiated as the bright white area in the center due to its lack of defects. Using high-resolution TEM (HRTEM) (Figure 3c), we can observe that despite its porous nature, the shell layer is still monocrystalline due to the regular lattice spacing across the nanowire. Furthermore, we do not observe any distortion in the selected area electron diffraction (SAED) pattern (Figure 3d), suggesting that the core and shell are oriented the same way despite being grown from different growth steps.

For the **pn** structure, a similar pattern is observed. From the TEM image (Figure 3e), we can see a darker core while the shell layer is lighter due to the difference in thickness. We can see some white spots in the core due to the void formation from doping. This is supported by the STEM image (Figure 3f), where the voids are also visible only in the core region, while the shell is clean. We do not get as clear a contrast from the voids in this case due to the presence of the clean shell layer. Similarly to the **np** sample, the HRTEM image (Figure 3g) also suggests that the structure is monocrystalline due to the regular lattice spacing. Furthermore, in the SAED pattern (Figure 3h), no distortion is observed despite the multiple growth steps.

In order to characterize the electrical properties of these homojunction films, 100 nm of ITO was deposited on top of the nanowires to form a top electrode. In both the **np** and **pn** samples, the bottom (i.e., the core) was under forward bias. In both samples, we observe rectification consistent with p−n junction behavior (Figure 4a). The **pn** sample has a turn on voltage of about 3 V, while the **np** device has a turn on voltage of about 2.5 V. There is also a noticeable amount of leakage when the devices are under reverse bias. Because of the way the sample is grown, there may be some contact between the shell layer and the bottom electrode. No patterning is used during growth of the core nanowire, so there is potentially exposed seed layer/electrode in between the nanowires. When the shell layer grows and backfills that space, it is possible for it to extend
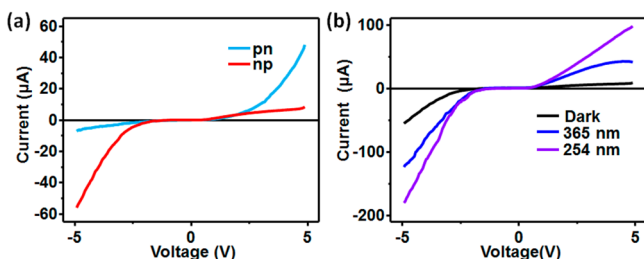
Figure 4. (a) I−V curves of the core−shell bulk homojunction film. In both cases, the bottom (i.e., the core) is under positive forward bias. Opposite rectification behavior is observed showing that both structures formed p−n junctions. (b) Photoresponse of the **np** film when exposed to a lamp under two different wavelengths of light, 254 and 365 nm.

Table 1. Responsivity at Different Driving Voltages for 365 and 254 nm Wavelength Light[a]

voltage (V)	365 nm	254 nm
1	0.024	0.015
2	0.089	0.058
3	0.158	0.114
4	0.203	0.174
5	0.425	0.318

[a]Units are A/W.

all the way to the seed layer, causing a short. This has been mitigated experimentally by allowing the core layer to grow for longer periods of time, which causes the nanowires to coalesce at the root, as can be seen from the cross-sectional SEM images in Figure 1. Because of the random nature of nucleation and growth, this does not completely eliminate the issue, leading to some shorting and thus leakage. Lithography techniques such as e-beam lithography or photolithography were considered to grow patterned ZnO nanowires for this investigation. However, the common photoresists used for these techniques, PMMA and SU8 were not compatible with high ammonia concentration used in the growth solution, which would cause them to swell and peel off the substrate. For future investigations, much more elaborate patterning techniques may need to be considered for investigating this growth method.

The photoresponse of the **np** device was investigated using an ultraviolet lamp. Because of the band gap of ZnO (∼3.44 eV), it should primarily absorb these wavelengths. The lamp had two different wavelength settings with different power levels at 0.66 mW/cm^2 at 365 nm and 1.61 mW/cm^2 at 254 nm. From the IV curves, it can be seen that the induced photocurrent causes the conductivity to increase in the device under both forward and reverse bias (Figure 4), suggesting that photoconduction may play a dominant role in this device's photodetecting behavior. Because the energy density of the 254 nm light is higher, a stronger response is observed. The standard method of normalizing photoresponse over different intensities is the responsivity term R[31] defined as

$$R = \frac{I_{light} - I_{dark}}{P_{light}}$$

where I_{light} and I_{dark} are the current under illumination and in the dark, respectively, and P_{light} is the power of the light source. With an active area of 0.25 cm^2, the calculated responsivity for the two light sources at a driving voltage of 1 V (reverse bias) was 0.024 and 0.015 A/W for the 365 and 254 nm light, respectively, so the sensitivity is on a similar order of magnitude for both wavelengths. By increasing the driving voltage, the responsivity can be increased as summarized in Table 1. This was increased up to 0.425 A/W at a voltage of 5 V putting it on par with commercially available Si based photodiodes. Similar patterns were observed for the **pn** sample (Figure S-2).

In conclusion, ZnO core−shell homojunction structures were grown using a low temperature, solution based hydrothermal method. By combining growth methods for fine wires and dense films, a homojunction structure with a high surface

area to volume ratio was produced. From microscopy investigations, despite the further changes in growth solution parameters, the telltale signs of doping, i.e., voids caused by antimony integration are still present, showing the further flexibility of this technique. Furthermore, the multistep growth used still produces single crystalline nanowires. By performing simple optoelectronic measurements, in the ultraviolet range, this device shows potential for photodetection. There is still room for refinement in both the growth to reduce the shorting between the shell layer and the substrate and in other potential optoelectronic applications such as light emission, which will be considered for future investigations.

■ ASSOCIATED CONTENT

Ⓢ Supporting Information

The Supporting Information is available free of charge on the ACS Publications website at DOI: 10.1021/acsami.5b11034.

  SEM images of n and p-type ZnO nanowire films and photoresponse behavior of the **pn** film (PDF)

■ AUTHOR INFORMATION

Corresponding Authors
*E-mail: zlwang@gatech.edu.
*E-mail: FUKATA.Naoki@nims.go.jp.

Notes
The authors declare no competing financial interest.

■ REFERENCES

(1) Qian, F.; Gradečak, S.; Li, Y.; Wen, C.-Y.; Lieber, C. M. Core/Multishell Nanowire Heterostructures as Multicolor, High-Efficiency Light-Emitting Diodes. *Nano Lett.* **2005**, 5 (11), 2287−2291.

(2) Tian, B.; Zheng, X.; Kempa, T. J.; Fang, Y.; Yu, N.; Yu, G.; Huang, J.; Lieber, C. M. Coaxial Silicon Nanowires as Solar Cells and Nanoelectronic Power Sources. *Nature* **2007**, 449 (7164), 885−889.

(3) Hua, B.; Motohisa, J.; Kobayashi, Y.; Hara, S.; Fukui, T. Single GaAs/GaAsP Coaxial Core−Shell Nanowire Lasers. *Nano Lett.* **2009**, 9 (1), 112−116.

(4) Wang, K.; Chen, J.; Zhou, W.; Zhang, Y.; Yan, Y.; Pern, J.; Mascarenhas, A. Direct Growth of Highly Mismatched Type II ZnO/ZnSe Core/Shell Nanowire Arrays on Transparent Conducting Oxide Substrates for Solar Cell Applications. *Adv. Mater.* **2008**, 20 (17), 3248−3253.

(5) Wu, Z.; Zhang, Y.; Zheng, J.; Lin, X.; Chen, X.; Huang, B.; Wang, H.; Huang, K.; Li, S.; Kang, J. An All-Inorganic Type-II Heterojunction Array with Nearly Full Solar Spectral Response Based on Zno/ZnSe Core/Shell Nanowires. *J. Mater. Chem.* **2011**, 21 (16), 6020−6026.

(6) Chen, Y.-J.; Zhang, F.; Zhao, G.-g.; Fang, X.-y.; Jin, H.-B.; Gao, P.; Zhu, C.-L.; Cao, M.-S.; Xiao, G. Synthesis, Multi-Nonlinear Dielectric Resonance, and Excellent Electromagnetic Absorption Characteristics of Fe_3O_4/ZnO Core/Shell Nanorods. *J. Phys. Chem. C* **2010**, *114* (20), 9239−9244.

(7) Dao, T.; Dang, C.; Han, G.; Hoang, C.; Yi, W.; Narayanamurti, V.; Nagao, T. Chemically Synthesized Nanowire TiO_2/ZnO Core-Shell pn Junction Array for High Sensitivity Ultraviolet Photodetector. *Appl. Phys. Lett.* **2013**, *103* (19), 193119.

(8) Law, M.; Greene, L. E.; Radenovic, A.; Kuykendall, T.; Liphardt, J.; Yang, P. $ZnO−Al_2O_3$ and $ZnO−TiO_2$ Core−Shell Nanowire Dye-Sensitized Solar Cells. *J. Phys. Chem. B* **2006**, *110* (45), 22652−22663.

(9) Pradhan, B.; Batabyal, S. K.; Pal, A. J. Rectifying Junction in a Single ZnO Vertical Nanowire. *Appl. Phys. Lett.* **2006**, *89* (23), 233109.

(10) Hoffmann, S.; Bauer, J.; Ronning, C.; Stelzner, T.; Michler, J.; Ballif, C.; Sivakov, V.; Christiansen, S. H. Axial p-n Junctions Realized in Silicon Nanowires by Ion Implantation. *Nano Lett.* **2009**, *9* (4), 1341−1344.

(11) Li, G.; Sundararajan, A.; Mouti, A.; Chang, Y.-J.; Lupini, A. R.; Pennycook, S. J.; Strachan, D. R.; Guiton, B. S. Synthesis and Characterization of p-n Homojunction-Containing Zinc Oxide Nanowires. *Nanoscale* **2013**, *5* (6), 2259−2263.

(12) Chiu, H.-M.; Chang, Y.-T.; Wu, W.-W.; Wu, J.-M. Synthesis and Characterization of One-Dimensional Ag-Doped ZnO/Ga-Doped ZnO Coaxial Nanostructure Diodes. *ACS Appl. Mater. Interfaces* **2014**, *6* (7), 5183−5191.

(13) Nguyen, X. S.; Tay, C. B.; Fitzgerald, E. A.; Chua, S. J. ZnO Coaxial Nanorod Homojunction UV Light-Emitting Diodes Prepared by Aqueous Solution Method. *Small* **2012**, *8* (8), 1204−1208.

(14) Ko, K. Y.; Kang, H.; Park, J.; Min, B.-W.; Lee, H. S.; Im, S.; Kang, J. Y.; Myoung, J.-M.; Jung, J.-H.; Kim, S.-H.; Kim, H. Zno Homojunction Core−Shell Nanorods Ultraviolet Photo-Detecting Diodes Prepared by Atomic Layer Deposition. *Sens. Actuators, A* **2014**, *210*, 197−204.

(15) Duan, L.; Wang, P.; Zhang, W.; Yu, X.; Fan, J.; Wei, F. Zno Homojunction Ultraviolet Photodetector Based on p-Type Dual-Doped Film and n-Type Nanorods. *Chem. Phys. Lett.* **2015**, *618*, 123−126.

(16) Zhang, S. B.; Wei, S. H.; Zunger, A. Intrinsic n-Type Versus p-Type Doping Asymmetry and the Defect Physics of ZnO. *Phys. Rev. B: Condens. Matter Mater. Phys.* **2001**, *63* (7), 075205.

(17) Van de Walle, C. G. Hydrogen as a Cause of Doping in Zinc Oxide. *Phys. Rev. Lett.* **2000**, *85* (5), 1012−1015.

(18) Fan, J. C.; Sreekanth, K. M.; Xie, Z.; Chang, S. L.; Rao, K. V. p-Type ZnO Materials: Theory, Growth, Properties and Devices. *Prog. Mater. Sci.* **2013**, *58* (6), 874−985.

(19) Lu, M.-P.; Lu, M.-Y.; Chen, L.-J. p-Type ZnO Nanowires: From Synthesis to Nanoenergy. *Nano Energy* **2012**, *1* (2), 247−258.

(20) Lany, S.; Zunger, A. Anion Vacancies as a Source of Persistent Photoconductivity in II-VI and Chalcopyrite Semiconductors. *Phys. Rev. B: Condens. Matter Mater. Phys.* **2005**, *72* (3), 035215.

(21) Wang, F.; Seo, J.-H.; Bayerl, D.; Shi, J.; Mi, H.; Ma, Z.; Zhao, D.; Shuai, Y.; Zhou, W.; Wang, X. An Aqueous Solution-Based Doping Strategy for Large-Scale Synthesis of Sb-Doped ZnO Nanowires. *Nanotechnology* **2011**, *22* (22), 225602.

(22) Yankovich, A. B.; Puchala, B.; Wang, F.; Seo, J. H.; Morgan, D.; Wang, X. D.; Ma, Z. Q.; Kvit, A. V.; Voyles, P. M. Stable p-Type Conduction from Sb-Decorated Head-to-Head Basal Plane Inversion Domain Boundaries in ZnO Nanowires. *Nano Lett.* **2012**, *12* (3), 1311−1316.

(23) Pradel, K. C.; Wu, W. Z.; Zhou, Y. S.; Wen, X. N.; Ding, Y.; Wang, Z. L. Piezotronic Effect in Solution-Grown p-Type ZnO Nanowires and Films. *Nano Lett.* **2013**, *13* (6), 2647−2653.

(24) Pradel, K. C.; Wu, W.; Ding, Y.; Wang, Z. L. Solution-Derived ZnO Homojunction Nanowire Films on Wearable Substrates for Energy Conversion and Self-Powered Gesture Recognition. *Nano Lett.* **2014**, *14* (12), 6897−6905.

(25) Wang, Z. L. Oxide Nanobelts and Nanowires - Growth, Properties and Applications. *J. Nanosci. Nanotechnol.* **2008**, *8* (1), 27−55.

(26) Wang, Z. L. ZnO Nanowire and Nanobelt Platform for Nanotechnology. *Mater. Sci. Eng., R* **2009**, *64* (3−4), 33−71.

(27) Briscoe, J.; Dunn, S. Piezoelectric Nanogenerators - A Review of Nanostructured Piezoelectric Energy Harvesters. *Nano Energy* **2015**, *14*, 15−29.

(28) Zhang, Y.; Liu, Y.; Wang, Z. L. Fundamental Theory of Piezotronics. *Adv. Mater.* **2011**, *23* (27), 3004−3013.

(29) Wen, X.; Wu, W.; Pan, C.; Hu, Y.; Yang, Q.; Lin Wang, Z. Development and Progress in Piezotronics. *Nano Energy* **2015**, *14*, 276−295.

(30) Tian, Z. R.; Voigt, J. A.; Liu, J.; McKenzie, B.; McDermott, M. J.; Rodriguez, M. A.; Konishi, H.; Xu, H. Complex and Oriented ZnO Nanostructures. *Nat. Mater.* **2003**, *2* (12), 821−826.

(31) Baeg, K.-J.; Binda, M.; Natali, D.; Caironi, M.; Noh, Y.-Y. Organic Light Detectors: Photodiodes and Phototransistors. *Adv. Mater.* **2013**, *25* (31), 4267−4295.